Journal of Electroanalytical Chemistry 784 (2017) 33–40

Contents lists available at ScienceDirect

Journal of Electroanalytical Chemistry

journal homepage: www.elsevier.com/locate/jelechem

Analysis of the hydrogen electrode reaction mechanism in thin-layer cells. 3. Study of hydrogen electro-oxidation by scanning electrochemical microscopy

Mariela A. Brites Helú, José L. Fernández *

Programa de Electroquímica Aplicada e Ingeniería Electroquímica (PRELINE), Facultad de Ingeniería Química, Universidad Nacional del Litoral, Santiago del Estero 2829, (S3000AOM) Santa Fe, Santa Fe, Argentina

ARTICLE INFO

Article history:
Received 1 September 2016
Received in revised form 31 October 2016
Accepted 28 November 2016
Available online 5 December 2016

Keywords:
Hydrogen oxidation reaction
Scanning electrochemical microscopy
Kinetic analysis
Thin-layer cell
Reaction mechanism

ABSTRACT

Scanning electrochemical microscopy (SECM) in the feedback mode was used to analyze the complete mechanism of the hydrogen oxidation reaction (*hor*). A general SECM equation was proposed to carry out the kinetic analysis of the dependences of the tip current (i_T) on the substrate potential (E_S) and on the tip-substrate distance (d). This SECM equation involves the contribution of a thin-layer cell (TLC) with no aprioristic restrictions about the reaction mechanism. A dependence of the TLC current on E_S previously developed for the *hor* operating through the Tafel-Heyrovsky-Volmer mechanism was included in the proposed SECM model. The domain of conditions where the equation properly reproduces the SECM responses was determined by contrasting the calculated $i_T(E_S, d)$ dependences with simulated curves obtained by a numerical method using varied kinetic and geometric parameters. The experimental conditions where the model can be used were explored by analyzing the *hor* on Pt. The present treatment provides a versatile tool for the application of SECM to the kinetic and mechanistic analysis of the *hor*, which can be easily adapted for the analysis of any multi-step electrocatalyzed reaction on infinite substrates.

1. Introduction

Scanning electrochemical microscopy (SECM) is a powerful electrochemical technique for the analysis of reaction mechanisms of electrocatalyzed reactions [1–3]. The great spatial resolution of this technique allows to restrict the kinetic analysis over confined submicrometer-sized domains of a macroelectrode and to achieve high mass transport rates (equivalent to those attained with micro- and nanoelectrodes). These properties make SECM (and its variants) an exceptional tool to analyze the effects of the surface state on reactions electrocatalyzed by heterogeneous electrode surfaces (i.e. structural [4–6], conformational [7,8], and compositional [9–11] effects). The technique has already been employed to study mechanistic aspects of a number of emblematic reactions in Electrocatalysis, which in general involve several elementary steps and the participation of one or more adsorbed intermediates, as are the hydrogen electrode reaction (HER) and the oxygen electrode reaction (OER) [1,2]. More specifically, the HER was studied by SECM in different operation modes, both to analyze its cathodic branch, the hydrogen evolution reaction (*her*) [12–17], and its anodic branch, the hydrogen oxidation reaction (*hor*) [7,10,17–27]. This last one (which is defined in acid media by Eq. (1)), is technologically important in energy conversion systems such as hydrogen-based fuel cells [28] where it operates on the anode under mixed control in the highly demanding mass-transport optimized conditions of real devices. Thus, the *hor* mechanism and kinetics play important roles in the anode performance. Besides, the knowledge of mechanisms related with poisoning by CO or impurities in the fuel, and with the tolerance to poisoning by cooperative effects still requires deeper investigations.

$$H_{2(g)} \leftrightarrows 2H^+ + 2e^- \quad (1)$$

Under these premises, the *hor* on different types of electrodes was analyzed using both feedback-based and generation collection modes. Bard and co-workers [18] were the first to analyze the *hor* by SECM pointing to understand the metal oxidation and adsorption of anions at high overpotentials. Contemporarily, Hillier and co-workers reported a kinetic analysis of the *hor* in the presence of CO on polycrystalline Pt [19,21], on Pt nanoparticle ensembles [20], and on combinations of Pt, Ru and Mo through combinatorial studies [22]. Furthermore, Zoski [23] carried out a kinetic study of the *hor* on polycrystalline Pt, Ir and Rh using feedback-based approach curves to obtain the exchange current densities on these metals. More recently, studies of the *hor* on multimetallic catalysts [10,24], supported nanoparticle arrays [17,25] and single nanoparticles [7] were reported. These works proved the

* Corresponding author.
E-mail address: jlfernan@fiq.unl.edu.ar (J.L. Fernández).

http://dx.doi.org/10.1016/j.jelechem.2016.11.065
1572-6657/

usefulness of SECM to reveal mechanistic details of this reaction even though they used approximate models to describe the *hor* mechanism (single step irreversible reaction [29]).

The kinetic analysis of electrode reactions by SECM in the feedback mode was recently comprehensively reviewed [30]. This type of study is usually carried out by correlation of experimental dependences of the tip current (i_T), or of its normalized value (I_T) respect to the current at infinite tip-substrate distance ($i_{T,\infty}$), on the normalized tip-substrate distance ($L = d/a$, where a is the tip radius) and on the substrate potential (E_S). The theoretical dependences to perform the correlations were generated by solving the diffusion equations for the SECM geometry and assuming a particular reaction mechanism for the substrate electrode reaction. On this sense, numerically simulated I_T-L-E_s curves for a single Butler-Volmer type electrode reaction at the substrate were earlier reported [31] and can be used to analyze single-step electrode reactions. Moreover, an analytical equation is available for an irreversible first-order reaction [29]. For the case of electrode reactions whose mechanisms involve more than one elementary step, these theoretical formalisms can be applied only in restricted potential ranges where one step becomes the rate determining step and a first-order dependence of the reaction rate on the reactant surface concentration is accomplished [32]. Thus, the rate constant (or the exchange current density) measured under these conditions is only an apparent indicator of the electrocatalytic activity and can hardly be related to the complete set of elementary kinetic parameters.

The *hor* operates by a three-step mechanism known as Tafel-Heyrovsky-Volmer (THV) mechanism, which in acid media involves steps (2) to (4) [32] (where S denotes an active site). The reaction proceeds simultaneously by two independent routes, which are the Tafel-Volmer and the Heyrovsky-Volmer routes, respectively [33]. The contribution of each of these routes to the whole reaction rate depends on the relative values of the elementary kinetic parameters. Thus for example, experiments carried out on Pt rotating disk electrodes (RDEs) [34,35], nanoelectrode arrays [36,37], and ultramicroelectrodes (UMEs) [38, 39] in acid media demonstrated that the *hor* operates principally through the Tafel-Volmer route at low overpotentials (<0.2 V) and it reaches a kinetic limiting current (current plateau) before the Heyrovsky-Volmer route becomes significant. For a direct observation of the transition between both routes, the diffusion limiting current density must be large enough (for example that verified on sub-micrometer UMEs [38] or highly-dispersed ensemble electrodes [36]) to become significantly different to the kinetic limiting value.

$$H_{2(g)} + 2\,S \leftrightarrows 2SH_{ad}\ \text{Tafel} \tag{2}$$

$$H_{2(g)} + S \leftrightarrows SH_{ad} + H^+ + e^-\ \text{Heyrovsky} \tag{3}$$

$$SH_{ad} \leftrightarrows S + H^+ + e^-\ \text{Volmer} \tag{4}$$

Taking into account the advantageous mass-transport properties of SECM, it is clear that this technique is particularly useful for the examination of the *hor* mechanism and for the determination of its elementary kinetic parameters on any substrate material, but a proper theoretical model to correlate the experimental $I_T(E_S, L)$ curves should be used. On that sense, there were a few attempts to generate more general models by applying corrections to the ideal thin-layer cell (TLC) configuration [40,41], which can be rigorously solved for the particular mechanism of the analyzed reaction. Moreover, a formalism to analyze the *hor* on an ideal TLC was already reported [42]. Thus, by incorporating this formalism in the TLC-based SECM theoretical equations, it should be possible to develop a model to carry out the mechanistic analysis of this reaction and the quantification of the complete set of elementary rate constants. In this context, this work reports a general equation for the analysis of $I_T(E_S, L)$ dependences, which introduces the TLC contribution in such a way that any reaction mechanism occurring at the substrate can be accounted. This equation is applied to describe the SECM feedback both for a typical quasi-reversible reaction (to test it against a well-known case) and for analyzing the THV mechanism of the *hor*, and contrasted with results of numerical simulations to verify its descriptive capabilities. The use of this equation to correlate experimental results is shown and discussed.

2. Theory

2.1. Analytical model

2.1.1. General model

A recent model that incorporates the TLC contribution as a TLC current (i_{TLC}) into the dependence of I_T on E_S and on L was reported by Zoski et al. [40] to carry out SECM tip voltammetry experiments on reversible reactions. On the basis of this model, the analytical expression for I_T given by Eq. (5) is proposed here.

$$I_T(E_S, L) = I_{TLC}(E_S, L)\varphi(L) + I_{disk}(E_S, L, t) \tag{5}$$

The core of this equation is the dependence of the normalized TLC current ($I_{TLC} = i_{TLC}/i_{T,\infty}$) for the reaction under study (for example the *hor*) on E_S and on L. This is affected by a parameter $\varphi(L) = (4/\pi)L\beta(I^{PF}{}_T - I^{NF}{}_T)$, which guarantees the attainment of the positive and negative feedback normalized limiting currents ($I^{PF}{}_T$ and $I^{NF}{}_T$, respectively), where β is the correction factor due to the finite tip-sheath radius (r_g), which depends on the ratio $R_g = r_g/a$ [29].

The reaction at the microelectrode tip is the backward reaction of the substrate operating under diffusion control. Then, Eq. (5) also involves the term I_{disk} defined by Eq. (6), which incorporates the contribution of the diffusion-limiting current at the microelectrode tip at a distance L ($i_{T,L}$) normalized respect to $i_{T,\infty}$.

$$I_{disk}(E_S, L, t) = \left(\frac{i_{T,L}(E_S, L, t)}{i_{T,\infty}}\right) I_T^{NF}(L) = c(E_S, L, t) I_T^{NF}(L) \tag{6}$$

Note that $i_{T,L}$ can be approximated by $i_{T,L} = 4\beta FDC(L)a$ [40], where D is the diffusion coefficient of the tip reactant, $C(L)$ is the local concentration at the distance L of the tip reactant, which could depend on E_S and time (t), and F is the Faraday constant. Moreover, $i_{T,\infty} = 4\beta FDC^*a$, where C^* is the bulk concentration of the tip reactant. Thus, $i_{T,L}/i_{T,\infty}$ results equal to the dimensionless reactant concentration ($c = C(L)/C^*$) at the distance L. In fact, the radial diffusion toward the disk tip is affected by the blocking effect that the substrate causes at a certain distance L. In Eq. (6) this effect is accounted by $I^{NF}{}_T$ [40]. Over the E_S interval where the substrate reaction proceeds in the studied direction (opposite to the tip reaction) the tip reactant concentration should not be modified ($C = C^*$ for all L), so $c = 1$. However, over the E_S interval where the reaction proceeds at the tip and at the substrate in the same direction, the reactant concentration is modified by the substrate, producing a time-dependant concentration profile (so called "shielding effect" [43]). As the substrate is infinite, the mass transport of the reactant toward its surface is carried out by linear diffusion. Then, under shielding conditions the value of c depends on E_S, on L, and on t. Such $c(E_S,L,t)$ dependence is determined by the reaction rate at the substrate, which is governed by the kinetics of the reaction.

The mechanism and kinetics of the studied reaction defines the $I_{TLC}(E_S,L)$ and $c(E_S,L,t)$ dependences. Two different cases are presented in this work. The first case is the quasireversible single-step reaction, which is very well known and can be used as a model-system for testing Eq. (5). The second case, which is the actual focus of this work, is the *hor* operating through the THV mechanism (Eqs. (2)–(4)). In both cases, reported expressions for $I^{PF}{}_T$, $I^{NF}{}_T$ and β [29] were used.

2.1.2. Quasi-reversible single-step reaction

For a quasi-reversible single step oxidation reaction ($R \leftrightarrows O + e^-$) operating at the substrate, the $I_{TLC}(E_S,L)$ and $c(E_S,L,t)$ dependences

were previously reported [43]. These are rearranged in Eqs. (7) and (8) (for equal diffusion coefficients of O and R), where $\Theta = \exp[F(E_S - E^{ref}) / RT]$ (E^{ref} in this case is the standard potential of the reaction, E^0), $\Lambda = k^0 a/D_O$ (k^0 is the standard rate constant), and $\tau = D_O t/a^2$ is the normalized time.

$$I_{TLC}(E_S, L) = \frac{(\pi/4\beta)\Theta}{\Lambda\Theta^{\alpha} + (\Theta + 1)L} \tag{7}$$

$$c(E_S, L, \tau) = \frac{\Theta + \mathrm{erf}\left(\frac{L}{2\sqrt{\tau}}\right) + e^{\Lambda\left(\frac{1+\Theta}{\Theta^{\alpha}}\right)\left[L+\Lambda\left(\frac{1+\Theta}{\Theta^{\alpha}}\right)\tau\right]}\mathrm{erfc}\left(\frac{L}{2\sqrt{\tau}} + \Lambda\left(\frac{1+\Theta}{\Theta^{\alpha}}\right)\sqrt{\tau}\right)}{1+\Theta} \tag{8}$$

2.1.3. The hydrogen oxidation reaction

The $I_{TLC}(E_S,L)$ for the *hor* can be obtained by rearranging the *hor* TLC current density previously reported [42] and expressing it in terms of L and $i_{T,\infty}$, which results in Eq. (9). The involved parameters are the coverage of H_{ad} at a certain value of E_S (θ) and at the reference potential conditions (θ^e) [42], the normalized equilibrium elementary rates $V^e{}_i = v^e{}_i a / (D_{H+} C^*{}_{H+})$ (where i indicates the elementary step V,H,T) and the symmetry factor α of both electrochemical steps. The Frumkin adsorption isotherm introduces the term $\Gamma = \exp[u(\theta - \theta^e)]$ (where u is the Frumkin interaction parameter) and the symmetry factor of the adsorption process (λ) [35]. The reference potential involved in Θ is the reversible hydrogen electrode (E^{RHE}) at $C^*{}_{H+}$ and $P_{H2} = 1$ atm. The parameter ξ is defined as $\xi = D_{H+}C^*{}_{H+}/(2D_{H2}C^{ref}{}_{H2}) = C^*{}_{H+}/3.59 \times 10^{-4}$ ($dm^3\ mol^{-1}$) [44,45], where $C^{ref}{}_{H2}$ is the solubility of H_2 at $P_{H2} = 1$ atm. From theses equalities, both the $I_{TLC}(E_S,L)$ and the $\theta(E_S,L)$ dependences can be obtained.

$$I_{TLC} = \frac{\left(\frac{\pi}{4\beta}\right)\left[V^e_V\left(\frac{\theta}{\theta^e}\right)\Gamma + V^e_H\xi\left(\frac{1-\theta}{1-\theta^e}\right)\right]\Theta}{\Gamma^{\lambda}\Theta^{1-\alpha} + \left\{V^e_V\left(\frac{1-\theta}{1-\theta^e}\right) + V^e_H\left[\left(\frac{\theta}{\theta^e}\right)\Gamma - \xi\left(\frac{1-\theta}{1-\theta^e}\right)\Theta\right]\right\}L} = \frac{\left(\frac{\pi}{4\beta}\right)\left\{V^e_V\left(\frac{\theta}{\theta^e}\right)\Gamma\Theta^{\alpha} + V^e_T\Gamma^{-\lambda}\left[\left(\frac{\theta}{\theta^e}\right)^2\Gamma^2 - \xi\left(\frac{1-\theta}{1-\theta^e}\right)^2\right]\right\}}{\frac{\Gamma^{\lambda}}{2} + \left[V^e_V\left(\frac{1-\theta}{1-\theta^e}\right)\Theta^{\alpha-1} - V^e_T\Gamma^{-\lambda}\xi\left(\frac{1-\theta}{1-\theta^e}\right)^2\right]L} \tag{9}$$

On the other hand, the rigorous $c(E_S,L,t)$ analytical profile should also be derived by solving the hydrogen evolution reaction on the infinite substrate. This is a rather difficult problem if the complete mechanism is considered. However, an approximated expression can be obtained assuming a Butler-Volmer type dependence with an exchange current density ($j^o = Fv^o$) calculated with the contributions of all the elementary step rates [44]. To gain even more simplicity a linear concentration profile can be considered through the diffusion layer thickness (δ). Besides, taking into account the time-dependence of δ given by the Cottrell equation [46], $\delta = (\pi D_{H+}t)^{1/2}$, an approximate $c(E_S,L,t)$ dependence can be established by Eq. (10), valid for $L < (\pi\tau)^{1/2}$, where the term $I_S(E_S,t)$ is defined by Eq. (11) and $V^o = v^o a/(D_{H+}C^*{}_{H+})$.

$$c(E_S, L, \tau) = [1 - I_S(E_S, \tau)] + \left(\frac{L}{\sqrt{\pi\tau}}\right) I_S(E_S, \tau) \tag{10}$$

$$I_S(E_S, \tau) = \left(1 + \frac{\xi e^{2F\left(E_S - E^{ref}\right)/RT}}{2} + \frac{e^{2(1-\alpha)F\left(E_S - E^{ref}\right)/RT}}{2V^o\sqrt{\pi\tau}}\right) - \sqrt{\left(1 + \frac{\xi e^{2F\left(E_S - E^{ref}\right)/RT}}{2} + \frac{e^{2(1-\alpha)F\left(E_S - E^{ref}\right)/RT}}{2V^o\sqrt{\pi\tau}}\right)^2 - 1} \tag{11}$$

2.2. Simulations

Steady state $I_T(E_S,L)$ curves were simulated by an iterative explicit finite difference method [47,48] written in Fortran programming language. The SECM discrete model for carrying out the finite different method is identical to that previously reported and fully described elsewhere [40] with the tip operating under diffusion limiting conditions. The only difference is the boundary condition at the substrate surface, which relates the fluxes and concentrations of reactants and products at this location with the reaction mechanism. For a quasireversible reaction the reaction rate (v) was defined in term of the surface concentrations by the Butler-Volmer equation. For the *hor*, the THV mechanism was incorporated into the SECM model through the boundary condition given by Eqs. (12)–(15) [44], where $v(r)$, $v_i(r)$, $\theta(r)$ and $C^s{}_i(r)$ are the reaction rate, the elementary rates, the coverage of H_{ad} and concentrations of dissolved species at the substrate surface, respectively, at the radial coordinate r from the tip axial axis.

$$2v(r) = v_V(r) + v_H(r) = 2[v_H(r) + v_T(r)] = 2[v_V(r) - v_T(r)] \tag{12}$$

$$v_T(r) = \frac{v^e_T}{\Gamma(r)^{2\lambda}}\left[\left(\frac{C^s_{H_2}(r)}{C^{ref}_{H_2}}\right)\left(\frac{1-\theta(r)}{1-\theta^e}\right)^2 - \left(\frac{\theta(r)}{\theta^e}\right)^2\Gamma(r)^2\right] \tag{13}$$

$$v_H(r) = \frac{v^e_H\Theta^{\alpha-1}}{\Gamma(r)^{\lambda}}\left[\left(\frac{C^s_{H_2}(r)}{C^{ref}_{H_2}}\right)\left(\frac{1-\theta(r)}{1-\theta^e}\right)\Theta - \left(\frac{C^s_{H^+}(r)}{C^*_{H^+}}\right)\left(\frac{\theta(r)}{\theta^e}\right)\Gamma(r)\right] \tag{14}$$

$$v_V(r) = \frac{v^e_V\Theta^{\alpha-1}}{\Gamma(r)^{\lambda}}\left[\left(\frac{\theta(r)}{\theta^e}\right)\Gamma(r)\Theta - \left(\frac{C^s_{H^+}(r)}{C^*_{H^+}}\right)\left(\frac{1-\theta(r)}{1-\theta^e}\right)\right] \tag{15}$$

Time-based iterations were carried out from the initial conditions, and the steady-state situation at a certain pair of E_S and L values was set when no significant changes on time were detected for the calculated concentrations and coverage values. The calculations started from an anodic E_S value that was kept during a quiet time ($\tau_{qt} = 100$) and the E_S value was changed every steps of −0.05 V (for the quasireversible case) and of −0.02 V (for the THV case) with step times $\tau_{step} = 50$. It should be noted that for $E_S - E^{ref} < 0$ the shielding effect is important [43] and a true steady state cannot be reached. The computation of $v(r)$ and of $\theta(r)$ necessary for recalculation of the surface concentrations every cycle in the finite difference method was carried out by a Newton-Raphson iterative algorithm [49].

3. Experimental

3.1. Chemical and materials

Analytical grade lithium perchlorate, sulphuric acid (98%), and perchloric acid (70%) from Merck (Germany) were used as received. Water was deionized with an exchange resin, doubly distilled, and treated with a Purelab purifier (Elga Labwater, resistivity ≥18.2 MΩ cm). Compressed gases (Ar 99.998% and N_2 99.999%) were from Indura (Argentina). Glassy carbon (GC) plates (1 mm thick, type I) used as film supports were from Alfa Aesar (USA).

3.2. Instrumentation

Scanning electrochemical microscopy experiments were carried out using a home-built SECM instrument described elsewhere [45]. A sputter coater Emitech K500X (UK) operating at 2 kV with Ar at a pressure of 0.1 mbar, furnished with a Pt disk target, was used for metallization of GC substrates with Pt. A benchtop Scanning Electron Microscope PhenomWorld model PROX (The Netherlands) was used for acquisition of SEM images of backscattered electrons.

3.3. Electrodes

Disk-shaped SECM tips (diameter < 25 μm) were fabricated by heat-sealing sharpened Pt wires in borosilicate glass capillaries followed by polishing, as it was described elsewhere [50]. A Hg/calomel electrode in saturated KCl solution was used as reference electrode, but all potentials are referred to the Reversible Hydrogen Electrode (RHE) in the same solution and at 1 atm of H_2 pressure. A Pt wire (1 mm diameter) was used as counter-electrode. SECM substrates were GC-supported thin films of Pt deposited by sputtering at 30 mA for 4 min. These electrodes were electrochemically treated by cyclic voltammetry in 0.5 M H_2SO_4 between 0 V and 1.4 V vs. RHE until reproducible cyclic voltammograms (CVs) were obtained, which allowed the estimation of the electroactive areas from the adsorbed-hydrogen electro-desorption charge [51]. A 0.3-mm thick Pt foil (Vega & Camji, Argentina) was also used as a substrate in some SECM experiments.

3.4. SECM experiments

Steady-state $i_T(E_S)$ curves were measured at different tip-substrate distances on a Pt foil and on GC-supported Pt thin films using the H^+/H_2 mediator loop [18,48] in deareated solutions of $HClO_4$ (0.02 M and 0.005 M) with 0.1 M $LiClO_4$ as supporting electrolyte under a N_2 environment. A Pt tip was approached at a tip potential $E_T = -0.7$ V vs. RHE and $E_S = 0.4$ V vs. RHE, measuring the positive feedback current for the diffusion-limited proton reduction. The approach curves were properly fitted with the theoretical expression for total positive feedback, which allowed to know the tip-substrate distances during the acquisition of $i_T(E_S)$ curves. Once the tip was positioned at a certain tip-substrate distance, the steady state $i_T(E_S)$ curve was measured by a slow potentiodynamic scan at -1 mV s^{-1} of the substrate potential from anodic (0.7 V vs. RHE) to cathodic (-0.25 V vs. RHE) values while keeping the tip potential at -0.7 V vs. RHE. After acquisition of a complete $i_T(E_S)$ curve the solution was agitated by a gentle bubbling of N_2, the tip-substrate distance was changed, and a new curve was measured.

4. Results and Discussion

4.1. Analytical equation vs. simulations

4.1.1. Quasi-reversible reaction

$I_T(E_S,L)$ curves for a single-step quasi-reversible reaction were simulated using a wide range of normalized standard rate constants ($10^{-3} \le \Lambda \le 25$) in the interval $0.1 \le L \le 1$ and over an E_S range that involved the diffusion limiting current, the kinetically affected region, the negative feedback region (in cases where it existed), and the shielding region. The comparison of the most representative simulated curves (SCs) with those calculated (CCs) with the same conditions using Eqs. (5)–(8) is shown in Fig. 1. Moreover, the differences between simulated and calculated I_T values are included below the respective $I_T(E_S)$ dependencies (in the same scale) to have a better and more quantitative image of the discrepancies between the approximate TLC-based model and the numerical calculations.

For $L = 0.1$ (Fig. 1a) the agreement between SCs and CCs is globally very good for all Λ values. Only slight differences between them, never larger than 0.5, can be detected at the potentials where the current begins to rise from the negative feedback value. As it was previously pointed out [29], the description of the SECM feedback process by a TLC is very good for small L and large reaction rates, but may not be as good when these conditions are not accomplished. In line with this, it is verified that in cases where the feedback current is only slightly larger than the negative feedback (low reaction rate), the TLC current underestimates the positive feedback contribution. On the other hand, due to the small L value, the negative feedback current that should be evident in curves obtained with small Λ values is almost imperceptible.

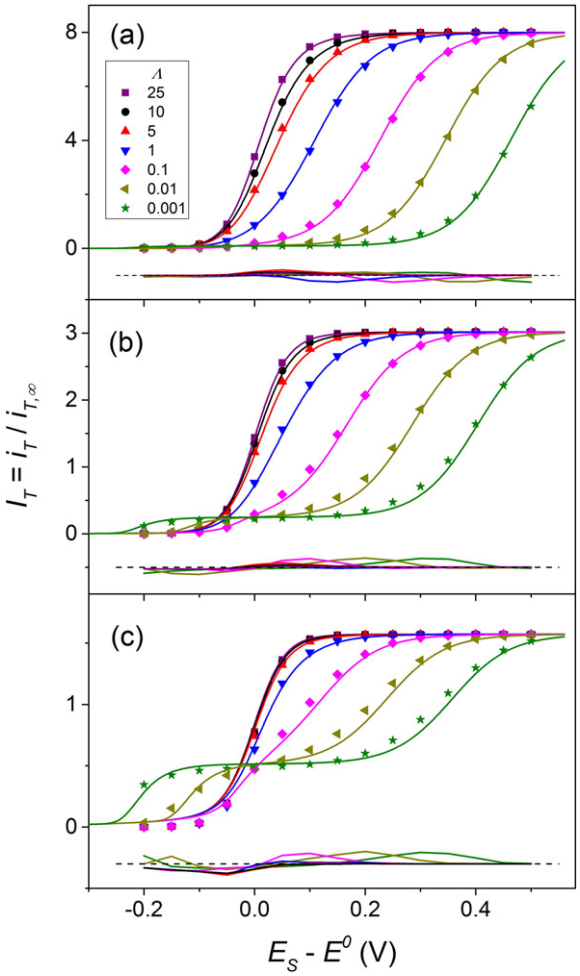

Fig. 1. Simulated (symbols) and calculated (lines) $I_T(E_S)$ dependencies for a single-step quasi-reversible reaction at $L = 0.1$ (a), 0.3 (b) and 0.8 (c) for the values of Λ indicated in the figure. $\tau = 50$. Lines below the $I_T(E_S)$ dependencies show the difference between simulated and calculated I_T values (dashed lines indicate null difference).

Something similar occurs with the current drops that proceed at $E_S < 0$ V due to the shielding effect. Fig. 1b ($L = 0.3$) and 1c ($L = 0.8$) show that as the distance increases the differences between SCs and CCs at low rates become more pronounced (as expected) but still smaller than 0.5 at any potential, and both the negative feedback and the shielding regions are better observed. While Eq. (5) leads to a proper description of the negative feedback limiting behavior, the description of the shielding region is poor, and becomes worst as L increases. This is not surprising since the current in the shielding region is strongly dependant on time and on the initial condition [40,43], which are not exactly the same in the compared SCs and CCs. Thus for example, in the SCs the initial condition for each simulated $I_T(E_S)$ point is the last concentration profile that resulted at the previous potential step (Section 2.2), while in the CCs the initial condition is the initial solution without perturbation. In spite of the described discrepancies between SCs and CCs, the agreement is acceptable and Eq. (5) could be used as a good approximation, particularly at the smaller distances ($L < 0.8$) and for the larger rate constants ($\Lambda \ge 0.1$) where the irreversible models may not be valid.

4.1.2. The hydrogen oxidation reaction

The $I_T(E_S)$ curves for the *hor* operating through the THV mechanism are affected by a group of five kinetic and adsorption parameters, without taking into account the symmetry factors. The analysis of the effect of all these parameters would be too extensive, and it actually was already carried out in a previous report [42]. Then, this work confines

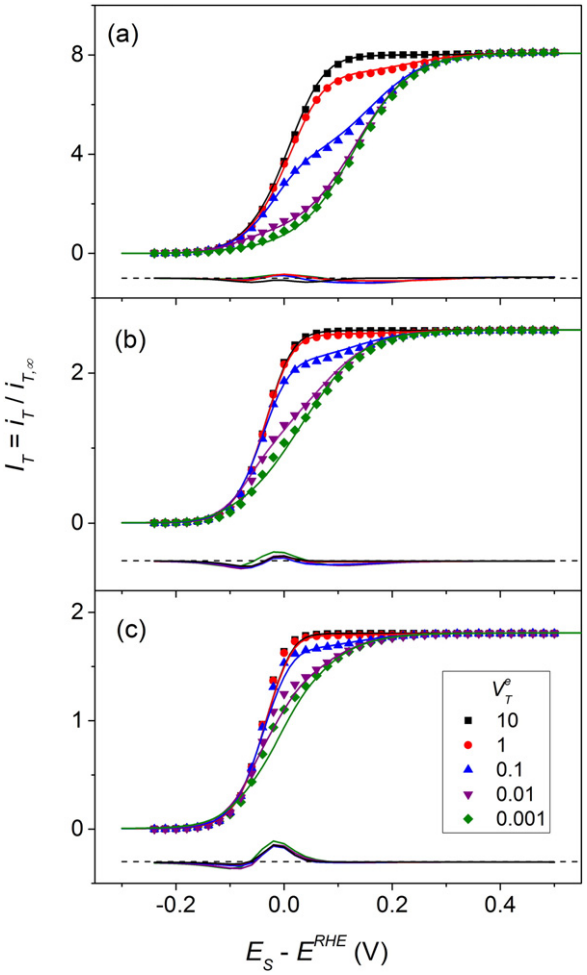

Fig. 2. Simulated (symbols) and calculated (lines) $I_T(E_S)$ dependencies for the *hor* operating through the THV mechanism at $L = 0.1$ (a), 0.37 (b) and 0.62 (c) for the values of V^e_T indicated in the figure. Other kinetic parameters: $V^e_V = 1$; $V^e_H = 0.01$; $\theta^e = 0.01$; $u = 0$; $\alpha = \lambda = 0.5$. $\tau = 50$. Lines below the $I_T(E_S)$ dependencies show the difference between simulated and calculated I_T values (dashed lines indicate null difference).

the kinetics conditions used for comparing SCs and CCs to values that are in the order of those reported for the *hor* on electrocatalysts based on noble metals that lead to high reaction rates. Thus, Fig. 2 shows some $I_T(E_S)$ SCs and CCs generated with Eqs. (5), (6), (9) and (10), that were obtained with the same kinetic parameters for varying L and Tafel equilibrium rates. As in the previous case, difference lines were also included below the $I_T(E_S)$ dependencies.

Similarly to the quasi-reversible case, good agreement between SCs and CCs was verified at small distances (typically $L < 0.4$), and only subtle discrepancies (differences smaller than 0.2) were detected over the potential interval between 0 and 0.2 V where the Tafel-Volmer kinetic limiting current [33,38] becomes evident. More pronounced differences are observed at larger distances, particularly over the potential interval of the shielding region (≤0 V). The deficient description of the shielding process at large distance may be caused not only by the differences of initial conditions between SCs and CCs (as in the quasi-reversible case), but also by the oversimplified linear model used for computing the time-dependant $c(L)$ dependence in Eq. (5), which in fact should be proportional to erfc(L) [43]. This analysis shows that Eq. (5) can be used with good accuracy to correlate experimental $I_T(E_S,L)$ curves for the *hor* measured on efficient electrocatalysts where the reaction is fast, as long as L is not larger than 0.5 ($I^{PF}_T > 2$). At increasing distances Eq. (5) becomes less accurate, particularly over the shielding region, but still its use could be acceptable up to $L \cong 1$. However, it is important to keep in mind that the analysis of a fast reaction like the *hor* only makes sense when it is performed at small distances where the mass transport rate is fast and the mechanistic features are fully revealed [42]. Finally, the effect of the other equilibrium rates of the elementary steps (V^e_V and V^e_H) are succinctly exemplified in Fig. 3, where the sensitivity of the $I_T(E_S)$ curves to these parameters at low L values is clearly realized.

4.2. Phenomenological issues affecting the analysis of hor $I_T(E_S,L)$ curves

The experimental $I_T(E_S,L)$ curves for the *hor* that are measured by SECM on any smooth substrate are affected by a number of phenomena that are not taken into account in the TLC-based model, which complicate the analysis. On the one hand, we recently demonstrated that electro-adsorption and surface diffusion of underpotentially adsorbed hydrogen (H_{UPD}) leads to a peak-shaped $I_T(E_S)$ dependence that is overlapped to the *hor* response [48]. The TLC-based mechanistic model obviously cannot reproduce this peak-shaped behavior. On the other hand, the evolution of H_2 from the substrate surface at cathodic potentials may involve the mass-transport of dissolved hydrogen not only by diffusion but also by convection, either natural or induced by nucleation of $H_{2(g)}$ bubbles. Such convective processes are hard to model and would strongly affect the $I_T(E_S,L)$ response over the shielding region. In order to visualize and address these effects, Fig. 4 shows $I_T(E_S)$ curves

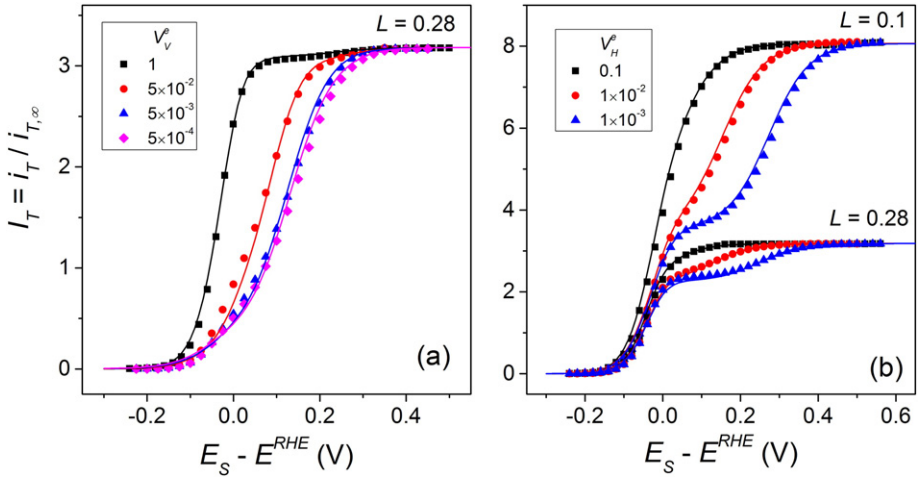

Fig. 3. Simulated (symbols) and calculated (lines) $I_T(E_S)$ dependencies for the *hor* operating through the THV mechanism showing the effects of V^e_V and of V^e_H. Kinetic parameters: $V^e_T = 0.5$; $\theta^e = 0.01$; $u = 0$; $\alpha = \lambda = 0.5$; (a) V^e_V indicated in the graph, $V^e_H = 0.005$; (b) $V^e_V = 1$, V^e_H indicated in the graph. $\tau = 50$.

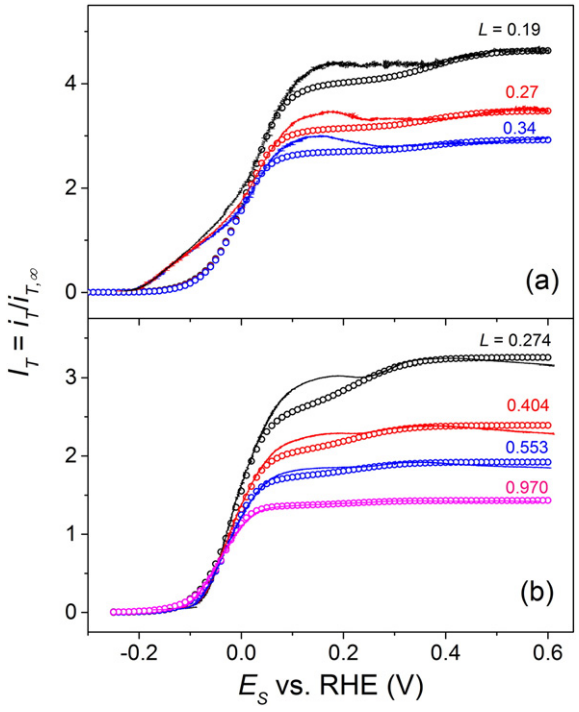

Fig. 4. Experimental $I_T(E_S)$ curves (lines) measured at different L values on a Pt foil in 20 mM [48] (a) and 5 mM (b) $HClO_4$ with 0.1 M $LiClO_4$. Tip conditions: (a) $a = 12.5$ μm, $R_g = 8$; (b) $a = 5.6$ μm, $R_g = 7$. Symbols are curves calculated with Eqs. (5), (6), (9) and (10) using the following kinetic parameters: (a) $v^e_V = 7.9 \times 10^{-7}$, $v^e_H = 2.3 \times 10^{-10}$, $v^e_T = 2.2 \times 10^{-7}$, $\theta^e = 0.18$, $u = 0.3$; (b) $v^e_V = 6.1 \times 10^{-7}$, $v^e_H = 2.1 \times 10^{-9}$, $v^e_T = 1.9 \times 10^{-7}$, $\theta^e = 0.18$, $u = 0.3$. v^e_i in mol cm^{-2} s^{-1}.

measured on a Pt foil in solutions with two different proton concentrations, and the best possible correlations with Eqs. (5), (6), (9) and (10).

The surface diffusion peaks are observed in both cases over $E_S > 0$ V vs. RHE, and the detrimental effects that they cause in the fitting ability are clearly pictured. This parallel surface process hampers the analysis of the *hor* with this model (and with any other SECM kinetic model) on continuous substrates that have the ability to adsorb H_{UPD}, such as Pt or the other noble metals. Such problem could probably be overcome either by limiting the substrate area to the region underneath the tip (using a finite substrate) or by using a discontinuous film supported on an inert conductor, with secluded surface domains that are unable to exchange adsorbed species by surface diffusion among them.

Another effect that is evident over the cathodic potentials is caused by the mass transport of dissolved H_2 from the substrate. It is clear that the concentration of proton plays an important role in this process. The observed fact is that when C^*_{H+} is not low enough (as in Fig. 4a, where $C^*_{H+} = 20$ mM) the experimental currents over the cathodic region are much larger than those expected for a pure diffusional process. However, when C^*_{H+} is small (as in Fig. 4b, where $C^*_{H+} = 5$ mM), the diffusional model reproduces very well the experimental $I_T(E_S)$ curve over this potential region. Even though generation of bubbles was not visually verified during the experiments, they still may be formed with undetectable nanometer sizes [52] and may add convective mechanisms to the H^+ mass transport. It was demonstrated that the generation of H_2 bubbles can be avoided on a microelectrode by working at low H^+ concentrations (typically $C^*_{H+} < 50$ mM for a 25-μm diameter disk [18]), since rapid removal of dissolved H_2 from the surface is attained by radial diffusion. However, such value becomes much smaller on an infinite substrate where diffusion is slow and C^s_{H2} may reach the critical oversaturation values required to nucleate bubbles. Diffusion-controlled voltammetric profiles for hydrogen evolution on macroelectrodes were reported for solutions with proton concentrations not larger than 10 mM [53,54]. Then, it is quite probable that the large deviations observed in the shielding region in Fig. 4a but not observed in Fig. 4b are caused by convective and/or resistive effects of $H_{2(g)}$ nanobubbles generated on the substrate surface.

Finally, a decrease of the diffusion-limiting feedback current is detected at very anodic potentials, which shifts to less anodic potentials as the proton concentration decreases. This deactivation is caused by electro-oxidation of Pt, which inhibits the *hor* [18,55]. While it would be possible to incorporate this inhibition process into the TLC-based *hor* model [55], this was not done in this work. Thus, the analysis of $I_T(E_S)$ curves is constrained to the potential interval where no inhibition by electro-oxidation is detected.

4.3. Analysis of the hor on metallic thin films by SECM

4.3.1. Characterization of metallic thin films

The GC-supported Pt films that were obtained by sputtering were mounted in the SECM cell exposing a geometric electrode area of 0.38 cm^2 (7-mm diameter) and their potential were cycled between 0.05 and 1.4 V vs. RHE at 0.1 V s^{-1} in 0.5 M H_2SO_4 solution. The cyclic voltammograms (CVs) varied from the first to the successive cycles but reached stable profiles after approximately 50 cycles, which are shown in Fig. 5. These CVs present the typical voltammetric behavior of carbon supported Pt in acid [39], where the H-adsorption/desorption peaks and the metal oxidation/reduction currents can be clearly identified. From the first ones it was possible to estimate the metal electroactive areas [51], resulting values of around 1.7 cm^2, or roughness factors between 4.5 and 4.8.

The morphology of the sputtered films after potential cycling in 0.5 M H_2SO_4 can be observed in the SEM micrographs shown in Fig. 6. Due to the great differences of the metal and carbon atomic weights, the images of backscattered electrons produces a sharp contrast between regions of these two materials, which allow to reveal the presence of film fractures and to distinguish the discontinuous nature of these films. Such cracked morphology is not detected in the as-prepared sputtered films and is surely caused by sintering of the sputtered metal nanoparticles induced by potential cycling in acid medium [54]. This type of morphology makes possible the SECM analysis of the *hor* on these Pt films without interferences from surface diffusion of H_{UPD}.

4.3.2. SECM analysis of the hor on GC-supported Pt thin films

The $I_T(E_S)$ curves measured at different tip-substrate distances on GC-supported Pt thin films previously described are shown in Fig. 7 (solid lines). They were measured in solutions with two different proton concentrations, 0.02 M (a) and 0.005 M (b), to illustrate the analysis in the presence (a) and absence (b) of convective effects over the shielding potential region. The best possible fittings with Eqs. (5), (6), (9) and (10) are also shown as open symbols.

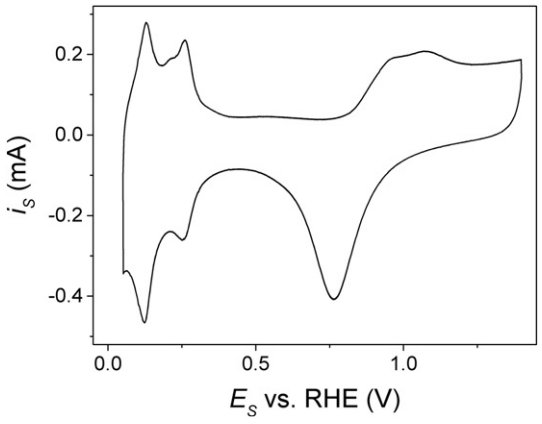

Fig. 5. Stabilized cyclic voltammogram of a typical GC-supported Pt thin film studied in this work, in 0.5 M H_2SO_4. Scan rate: 0.1 V s^{-1}.

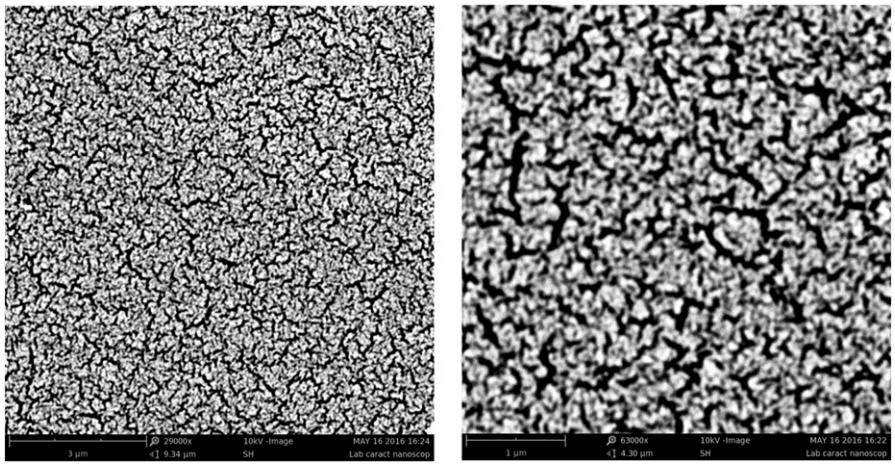

Fig. 6. SEM micrographs of backscattered electrons obtained at 29000× (left) and 63000× (right) on the glassy carbon supported Pt thin films studied in this work. Scale bars indicate 3 μm (left) and 1 μm (right).

The GC support is an inert material unable to electrocatalyze the *hor*. Then, only negative feedback is verified on pure GC over the anodic potential ranges, and shielding due to hydrogen evolution is only detected at $E_S < 0.5$ V vs. RHE (results not shown). The discontinuous structure of the film hampers the surface diffusion of H_{UPD} from the tip-affected area to the tip-unaffected region, causing the vanishing of the consequent peaks that should be expected between 0 and 0.3 V vs. RHE [48]. This problem was thus overcome by working with this type of substrate. However, the convective/resistive effects caused by bubble generation on the substrate surface at cathodic potentials at the larger proton concentration, clearly evident in Fig. 7a, still are important and impede the analysis of the complete $I_T(E_S)$ curves. In spite of that, most of the anodic branch that is unaffected by the shielding can be correlated with the TLC-based model, allowing the estimation of the *hor* kinetic parameters shown in Table 1. In contrast, all the $I_T(E_S)$ curves measured at a low H^+ concentration (Fig. 7b) were free of convective and surface diffusion effects, and were properly correlated over the whole potential range with the TLC-based model using a single set of *hor* kinetic parameters listed in Table 1. Overall, these parameters agree with those reported for the HER on polycrystalline Pt in similar pH conditions [44,45], and indicate the prevalence of the Tafel-Volmer route at low potentials. Nevertheless, it results surprising the apparent dependences of the equilibrium rates on the proton concentration. As the proton concentration falls, while the Volmer equilibrium rate decreases and the Tafel equilibrium rate remains almost unchanged (as expected [44]), the Heyrovsky equilibrium rate clearly grows almost one order of magnitude (in opposition to the expected dependence [44]). Such result was also visualized in the *hor* analysis of the Pt foil (Fig. 4) and was consistently observed in many other experiments carried out on similar Pt thin-films (not shown). Moreover, reported data of HER elementary rate constants as a function of pH show an increase of the Heyrovsky rate constant with decreasing proton concentration [44]. This unexpected trend should be the focus of a deeper analysis.

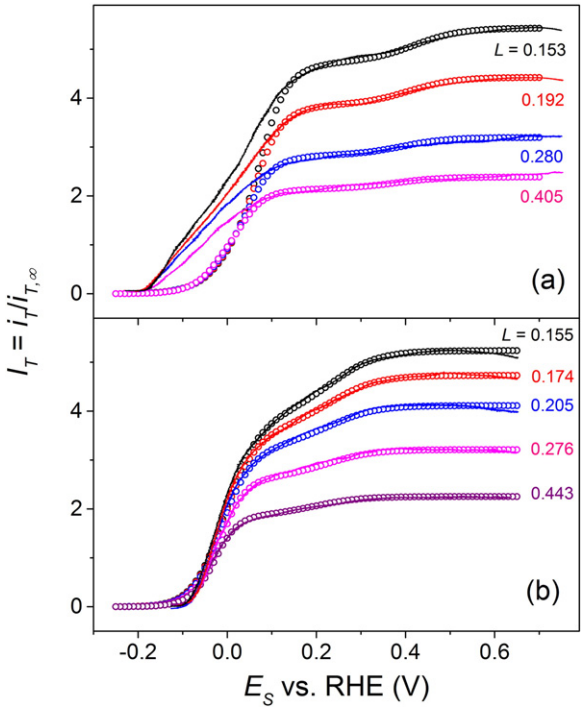

Fig. 7. Experimental $I_T(E_S)$ curves (lines) measured at different L values on GC-supported Pt thin films in 20 mM (a) and 5 mM (b) $HClO_4$ with 0.1 M $LiClO_4$. Symbols are curves simulated with Eqs. (5), (6), (9) and (10), using the kinetic parameters listed in Table 1. Tip conditions: (a) $a = 6.7$ μm, $R_g = 8$; (b) $a = 12.1$ μm, $R_g = 3$.

5. Conclusions

The TLC-based empirical equation proposed to analyze the $I_T(E_S,L)$ dependences is a versatile tool for the feedback-based SECM analysis of reactions with complex mechanisms. However, by contrasting the equation with numerical simulation for a single quasireversible reaction and for the *hor* operating through the THV mechanism, it was found that a number of conditions need to be accomplished to guarantee a good accuracy. The first input involved in the equation, which is the TLC contribution, properly represents the feedback process as long as the deviation of the SECM arrangement from the TLC configuration is not large. Thus, the equation has a good performance at L values typically smaller than 0.5 and for reactions that operate with large reaction rates. The second part involved in the proposed equation is the shielding contribution. Even though this is the least accurate term, it actually affects a part of the $I_T(E_S)$ curve that has little influence on the calculated kinetic parameters.

The kinetics of the *hor* was successfully studied on Pt substrates by analyzing $I_T(E_S)$ curves with a THV TLC contribution incorporated in

Table 1
Kinetic parameters resulting from correlations of SECM $I_T(E_S)$ curves for the *hor* shown in Fig. 7. v^e_i in mol s^{-1} cm^{-2}, u (in RT units) = 0.3, $\alpha = \lambda = 0.5$.

C_{H+} (mol dm^{-3})	v^e_V	v^e_H	v^e_T	θ^e
0.02	6.4×10^{-7}	2.1×10^{-10}	1.3×10^{-7}	0.181
0.005	4.3×10^{-7}	1.9×10^{-9}	1.1×10^{-7}	0.185

this equation. The analysis of the complete experimental $I_T(E_S)$ curve is only feasible when the proton concentration is smaller than 10 mM and when the substrate surface has a configuration that hampers the surface diffusion of H_{UPD} (for example a discontinuous film). Under these conditions the kinetic parameters of the *hor* mechanism can be properly calculated from the curve fittings. Thus, the elementary kinetic parameters were calculated from correlations of $I_T(E_S)$ curves measured on GC-supported Pt thin films, and resulted similar to those previously measured on polycrystalline Pt. However, when the first condition is not accomplished (too large proton concentration), the generation of small $H_{2(g)}$ bubbles from the substrate over the cathodic potential range produces convection, which makes impossible the correlation of the complete curves with the proposed model. However, this interference does not affect the fitting of the curves over the anodic region and the calculation of the *hor* kinetic parameters still is possible. Moreover, when surface diffusion of H_{ad} is not blocked (i.e. when using a continuous substrate), the consequent peaks from this process are overlapped to the anodic branch of the curve, impeding its correlation with the proposed equation.

Acknowledgements

This work was supported by Agencia Nacional de Promoción Científica y Tecnológica (ANPCyT) (PICT 2014 2001 and PICT-E 2014 0239), Consejo Nacional de Investigaciones Científicas y Técnicas (CONICET) (PIP 112-201101-00674) and Universidad Nacional del Litoral (CAI+D 501-201101-00333 LI).

References

[1] J. Rodríguez-López, C.G. Zoski, A.J. Bard, in: A.J. Bard, M.V. Mirkin (Eds.), Scanning Electrochemical Microscopy, second ed.CRC Press, Boca Raton 2012, pp. 525–568 (Chapter 16).
[2] C.G. Zoski, J. Electrochem. Soc. 163 (2016) H3088–H3100.
[3] Y. Li, X. Ning, Q. Ma, D. Qin, X. Lu, Trends Anal. Chem. 80 (2016) 242–254.
[4] B.D.B. Aaronson, S.C.S. Lai, P.R. Unwin, Langmuir 30 (2014) 1915–1919.
[5] K. Verbeken, L. Kestens, J.M.C. Mol, H. Terryn, Electrochim. Acta 116 (2014) 89–96.
[6] B.D.B. Aaronson, C.H. Chen, H. Li, M.T.M. Koper, S.C.S. Lai, P.R. Unwin, J. Am. Chem. Soc. 135 (2013) 3873–3880.
[7] J. Kim, C. Renault, N. Nioradze, N. Arroyo-Currás, K.C. Leonard, A.J. Bard, J. Am. Chem. Soc. 138 (2016) 8560–8568.
[8] A.G. Güell, N. Ebejer, M.E. Snowden, J.V. Macpherson, P.R. Unwin, J. Am. Chem. Soc. 134 (2012) 7258–7261.
[9] X. Chen, A.J.R. Botz, J. Masa, W. Schuhmann, J. Solid State Electrochem. 20 (2016) 1019–1027.
[10] Y.C. Weng, C.T. Hsieh, Electrochim. Acta 56 (2011) 1932–1940.
[11] J.L. Fernández, D.A. Walsh, A.J. Bard, J. Am. Chem. Soc. 127 (2005) 357–365.
[12] A.R. Kucernak, P.B. Chowdhury, C.P. Wilde, G.H. Kelsall, Y.Y. Zhu, D.E. Williams, Electrochim. Acta 45 (2000) 4483–4491.
[13] F. Li, P. Bertoncello, I. Ciani, G. Mantovani, P.R. Unwin, Adv. Funct. Mater. 18 (2008) 1685–1693.
[14] F. Li, I. Ciani, P. Bertoncello, P.R. Unwin, J. Zhao, C.R. Bradbury, D.J. Fermin, J. Phys. Chem. C 112 (2008) 9686–9694.
[15] K.C. Leonard, A.J. Bard, J. Am. Chem. Soc. 135 (2013) 15890–15896.
[16] H. Li, M. Du, M.J. Mleczko, A.L. Koh, Y. Nishi, E. Pop, A.J. Bard, X. Zheng, J. Am. Chem. Soc. 138 (2016) 5123–5129.
[17] S. Ahmed, S. Li, L. Petrik, V.M. Linkov, Anal. Sci. 20 (2004) 1283–1287.
[18] J. Zhou, Y. Zu, A.J. Bard, J. Electroanal. Chem. 491 (2000) 22–29.
[19] K. Jambunathan, B.C. Shah, J.L. Hudson, A.C. Hillier, J. Electroanal. Chem. 500 (2000) 279–289.
[20] S. Jarayaman, A.C. Hillier, Langmuir 17 (2001) 7857–7864.
[21] K. Jambunathan, A.C. Hillier, J. Electroanal. Chem. 524–525 (2002) 144–156.
[22] S. Jayaraman, A.C. Hillier, J. Phys. Chem. B 107 (2003) 5221–5230.
[23] C.G. Zoski, J. Phys. Chem. B 107 (2003) 6401–6405.
[24] G. Lu, J.S. Cooper, P.J. McGinn, J. Power Sources 161 (2006) 106–114.
[25] P.G. Nicholson, S. Zhou, G. Hinds, A.J. Wain, A. Turnbull, Electrochim. Acta 54 (2009) 4525–4533.
[26] Y.H. Yin, L. Niu, X.L. Cao, J. Chin. Chem. Soc. 56 (2009) 1092–1098.
[27] M. Parthasarathy, V.K. Pillai, J. Chem. Sci. 121 (2009) 719–725.
[28] F. Barbir, PEM Fuel Cells: Theory and Practice, second ed. Elsevier, Amsterdam, 2013 33–72 (Chapter 3).
[29] C. Lefrou, R. Cornut, Chem. Phys. Chem. 11 (2010) 547–556.
[30] S. Amemiya, in: A.J. Bard, M.V. Mirkin (Eds.), Scanning Electrochemical Microscopy, second ed.CRC Press, Boca Raton 2012, pp. 127–156 (Chapter 6).
[31] A.J. Bard, M.V. Mirkin, P.R. Unwin, D.O. Wipf, J. Phys. Chem. 96 (1992) 1861–1868.
[32] E. Gileadi, Electrode Kinetics for Chemists, Chemical Engineers, and Materials Scientists, VCH, New York, 1993 127–184 (Chapter F).
[33] M.R. Gennero de Chialvo, A.C. Chialvo, Phys. Chem. Chem. Phys. 6 (2004) 4009–4017.
[34] P.M. Quaino, M.R. Gennero de Chialvo, A.C. Chialvo, Phys. Chem. Chem. Phys. 6 (2004) 4450–4455.
[35] P.M. Quaino, M.R. Gennero de Chialvo, A.C. Chialvo, Electrochim. Acta 52 (2007) 7396–7403.
[36] M.A. Montero, M.R. Gennero de Chialvo, A.C. Chialvo, Electrochim. Acta 56 (2010) 756–761.
[37] E. Kemppainen, J. Halme, P.D. Lund, Phys. Chem. Chem. Phys. 18 (2016) 13616–13628.
[38] P.M. Quaino, J.L. Fernández, M.R. Gennero de Chialvo, A.C. Chialvo, J. Mol. Catal. A Chem. 252 (2006) 156–162.
[39] M.D. Arce, J.L. Fernández, M.R. Gennero de Chialvo, A.C. Chialvo, J. Electroanal. Chem. 642 (2010) 41–51.
[40] C.G. Zoski, C.R. Luman, J.L. Fernández, A.J. Bard, Anal. Chem. 79 (2007) 4957–4966.
[41] S. Amemiya, N. Nioradze, P. Santhosh, M.J. Deible, Anal. Chem. 83 (2011) 5928–5935.
[42] J.L. Fernández, J. Electroanal. Chem. 650 (2010) 90–97.
[43] C.G. Zoski, J.C. Aguilar, A.J. Bard, Anal. Chem. 75 (2003) 2959–2966.
[44] M.D. Arce, H.L. Bonazza, J.L. Fernández, Electrochim. Acta 107 (2013) 248–260.
[45] H.L. Bonazza, L.D. Vega, J.L. Fernández, J. Electroanal. Chem. 713 (2014) 9–16.
[46] A.J. Bard, L.R. Faulkner, Electrochemical Methods: Fundamentals and Applications, second ed. John Wiley & Sons, New York, 2001.
[47] J.L. Fernández, C. Hurth, A.J. Bard, J. Phys. Chem. B 109 (2005) 9532–9539.
[48] M.A. Brites Helú, H.L. Bonazza, J.L. Fernández, J. Electroanal. Chem. 775 (2016) 64–71.
[49] W.H. Press, B.P. Flannery, S.A. Teukolsky, W.T. Vetterling, Numerical Recipes, Cambridge University Press, Cambridge, 1986 240–273 (Chapter 9).
[50] H.L. Bonazza, J.L. Fernández, J. Electroanal. Chem. 650 (2010) 75–81.
[51] R. Woods, J. Electroanal. Chem. 49 (1974) 217–226.
[52] S.R. German, Q. Chen, M.A. Edwards, H.S. White, J. Electrochem. Soc. 163 (2016) H3160–H3166.
[53] M. Ciszkowska, Z. Stojek, S.E. Morris, J.G. Osteryoung, Anal. Chem. 64 (1992) 2372–2377.
[54] M.A. Brites Helú, M.R. Gennero de Chialvo, A.C. Chialvo, J.L. Fernández, J. Solid State Electrochem 18 (2014) 2233–2243.
[55] M.S. Rau, M.R. Gennero de Chialvo, A.C. Chialvo, J. Power Sources 229 (2013) 210–215.